Journal of Manufacturing Processes

Vacuum melting of compressed powders and hot rolling of the Ti-48Al-2Nb-0.7Cr-0.3Si intermetallic alloy: Mechanical properties and microstructural analysis

--Manuscript Draft--

Manuscript Number:	SMEJMP-D-22-03710R1
Article Type:	Full Length Article
Keywords:	powders; Microstructural refinement; Hot-pack rolling; intermetallic; -TiAl alloy
Corresponding Author:	Amogelang Bolokang SOUTH AFRICA
First Author:	Amogelang Bolokang
Order of Authors:	Amogelang Bolokang
	John Ellard
	Maria Mathabathe
	Chartles Siyasiya
Abstract:	The amalgamated effect of hot-rolling, rapid cooling and heat treatment on the grain refinement and the resultant mechanical properties of an intermetallic sheet of nominal composition Ti-48Al-2Nb-0.7Cr-0.3Si was investigated. The sheet of 4 mm thickness was fabricated by hot-pack rolling from the vacuum arc remelted (VAR) ingot using a conventional two-high rolling mill. After the final rolling pass, the canned specimen was rapidly cooled in the air to room temperature followed by heat treatment in the a+g region. The scanning electron microscopy (SEM) micrographs of the as-rolled sheet revealed slightly elongated grains of a typical “duplex (DP)” microstructure with a mean grain size of about 3 μm which grew to about 4 mm and became more equiaxed and homogeneous after heat treatment. Moreover, the EBSD micro-texture indicated a weak cube texture in the rolled + heat-treated sheet. Furthermore, the results from the profilometry-based indentation plastometry of the rolled + heat treated specimen illustrated the balanced and improved mechanical properties compared to the as-cast and as-rolled samples.
Opposed Reviewers:	

Vacuum melting of compressed powders and hot rolling of the as-cast Ti-48Al-2Nb-0.7Cr-0.3Si intermetallic alloy: Mechanical properties and microstructural analysis

J.J.M. Ellard[1], M.N. Mathabathe[2], C. Siyasiya[1], A.S. Bolokang[2,3,4]*

[1]Department of Material Science and Metallurgical Engineering, Faculty of Engineering, Built Environment and Information Technology, University of Pretoria, South Africa.

[2]Council of Scientific Industrial Research, Manufacturing cluster, Advanced Materials Engineering, Meiring Naude Road, P O Box 395 Pretoria, South Africa.

[3]Department of Physics, University of the Free State, P.O. Box 339, Bloemfontein, ZA9300, South Africa

[4]Department of Physics, University of the Western Cape, Private Bag X 17, Bellville 7535, South Africa

ABSTRACT

The amalgamated effect of hot-rolling, rapid cooling and heat treatment on the grain refinement and the resultant mechanical properties of an intermetallic sheet of nominal composition Ti-48Al-2Nb-0.7Cr-0.3Si was investigated. The sheet of 4 mm thickness was fabricated by hot-pack rolling from the vacuum arc remelted (VAR) ingot using a conventional two-high rolling mill. After the final rolling pass, the canned specimen was rapidly cooled in the air to room temperature followed by heat treatment in the $\alpha+\gamma$ region. The scanning electron microscopy (SEM) micrographs of the as-rolled sheet revealed slightly elongated grains of a typical “duplex (DP)” microstructure with a mean grain size of about 3 μm which grew to about 4 μm and became more equiaxed and homogeneous after heat treatment. Moreover, the EBSD micro-texture indicated a weak cube texture in the rolled + heat-treated sheet. Furthermore, the results from the profilometry-based indentation plastometry of the rolled + heat treated specimen illustrated the balanced and improved mechanical properties compared to the as-cast and as-rolled samples, and also those of similar alloy systems found in the literature.

***Keywords**:* Microstructural refinement; Hot-pack rolling; Intermetallic; γ-TiAl alloy

*Corresponding author.

E-mail addresses: sbolokang@csir.co.za (A.S. Bolokang), ellardjholy@gmail.com (J.J.M. Ellard), nmathabathe@csir.co.za (M.N. Mathabathe); Charles.siyasiya@up.ac.za.

1. Introduction

As the need for lighter alloys to replace the heavier ones in aerospace and automobile industries to reduce fuel consumption, noise, NOx emissions, and maintenance costs as well as improve performance continues to grow, γ-TiAl-based alloys remain the promising materials for high-temperature applications. The alloys were first implemented in a race sport engine in the year 2000 **[1]**. A decade later, the γ-TiAl-based alloy blades replaced Ni-based super-alloy blades in the last stage of the low-pressure turbine of a Boeing aircraft B747-8 engine **[2]**. Apart from their lightweight property, high-temperature strength, good resistance to corrosion and oxidation are the other important properties that led to the real commercial applications of the alloys **[3–7]**. It has been established that those γ-TiAl-based alloys with fine and homogeneous microstructures possess well-balanced properties **[8**,**9]**. Therefore, extensive research has been dedicated to alloy design methods and processing routes that yield fine microstructures viz.: Alloying with grain refiners such as boron to form TiB mono- or TiB_2 di-borides which act as nucleating sites in the melt during solidification **[10**–**13]**. However, precaution needs to be taken to avoid the formation of curvy borides as they have a strong effect on reducing the ductility of the alloy **[14]**. Secondly, heat treatment such as cyclic, rapid and multi-step processes have been successfully employed to several γ-TiAl-based alloy systems to refine their microstructures **[7**,**15**–**18]**. However, Schwaighofer et al.,**[7]** demonstrated that with heat treatment the resulting microstructural properties are not completely balanced i.e. the improvement in properties such as strength and creep resistance leads to reduced room temperature ductility. Apart from alloying and heat treatment, research has also demonstrated that thermo-mechanical treatments (hot-working) such as hot-forging **[19**,**20]**, hot-extrusion **[21]** and hot-rolling **[22**–**26]** are also capable of adjusting the microstructures of the alloys**.** Of all the existing methods of microstructural refinement, hot-working is regarded as the most attractive and efficient way of obtaining useful γ-TiAl-based products that possess optimised mechanical properties **[25]**. During hot-working, an increased dislocation density assists to refine coarse microstructure by activating recrystallization processes **[7]**. Tang et al., **[19]** reported a fine homogeneous

microstructure with a mean grain size of about 13 μm which was obtained through a multi-step non-canned forging process. In another study, Burtscher et al., **[21]** managed to refine the microstructure of Ti-43.3Al-4Nb-1Mo-0.1B (in at%) alloy to an average grain size of 1.8 μm using hot-extrusion. Excellent mechanical properties at room temperature such as hardness of 393 HV, yield strength of 1121 MPa and ultimate tensile strength of 1213 MPa were obtained from the resulting alloy. Despite these outstanding properties, the ambient temperature elongation for the alloy was found to be only 1.3 %. On γ-TiAl cast ingots fabrication Shen et al., **[25]** has shown that it is possible to induce a high Nb-TiAl based sheet of fine microstructure with an average grain size of about 15 μm using a hot-pack rolling process. The researchers reported that the fabricated sheet possessed about 600 MPa and 750 MPa as yield and ultimate tensile stresses respectively with an engineering strain of about 2.6 % at room temperature. However, this is applicable to high Nb containing γ-TiAl based alloys whose corresponding process parameters may not be suitable for the peritectic low Nb containing γ-TiAl alloys. In the case of the grain refinement of the peritectic-solidifying low Nb γ-TiAl sheets by rolling, there is little information in literature that describe the grain sizes attained and their corresponding mechanical properties. For instance, Clemens et al., **[27]** reported the characterisation and mechanical properties of Ti-48Al-2Cr sheet material fabricated by hot-rolling. Prior to the rolling process, the cast alloy was forged. The mean grain size after hot-rolling and subsequent vacuum annealing at 1000 °C for 2 hours was found to be around 19 μm. The tensile test of the resulting sheet at 25 °C revealed yield strength of 426 MPa, ultimate tensile strength of 515 MPa and a plastic strain of 2.0%. It is apparent that the mechanical properties of the sheet can be improved. As demonstrated by Burtscher et al., **[21]**, the finer the grain size of the alloy, the more improved mechanical properties. Therefore, there should be a suitable and cost-effective combination of fabrication processes which could be capable of producing a sheet material with refined grains that can result into balanced and improved mechanical properties from a modified second generation γ-TiAl-based ingot. In the present study, the microstructure of a γ-TiAl-based alloy sheet with nominal composition Ti-48Al-2Nb-0.7Cr-0.3Si produced by amalgamated effects of hot-rolling, rapid cooling and heat treatment was investigated. The ingot was fabricated by

vacuum arc remelting (VAR) of the uniaxially cold pressed precursor powders. The sheet was manufactured by direct hot-pack rolling of the cast ingot without intermediate thermo-mechanical processes such as hot isostatic pressing (HIPing) to reduce the processing cost.

2. Experimental work

The γ-TiAl-based cast ingot with a nominal composition of Ti-48Al-2Nb-0.7Cr-0.3Si (at.%) and dimensions 38 × 38 × 13 mm^3 was produced by vacuum arc remelting (VAR) through uniaxial compression of pure precursor powders. The vacuum used in the VAR electric arc melting furnace and the compression pressure in the pressing machine were 1×10^{-5} Torr and 380 MPa, respectively. The same fabrication procedure was reported in **[28–31].** The as-cast ingot was encapsulated in a 316 austenitic stainless-steel case of 45 × 45 × 15 mm^3. This was carried out because of the following main reasons: 1) to prevent cracking of the ingot due to the large temperature gradient between the hot ingot and the cold mill rolls; 2) to minimise oxygen uptake and heat loss in transit from the furnace to the rolling mill; 3) to provide a quasi-iso-pressure to the ingot during hot-rolling, which subjects it under a form of tri-axial pressing and ameliorate the yield and working efficiency **[32–34].** To avoid the bonding of the ingot and the case during the rolling process, the ingot-case interface was filled with zirconia powder **[25]**. The case was sealed by tungsten inert gas (TIG) welding. Finally, the sealed case was heated to 1280 °C for 30 min and then rolled on a two-high mill with rolls of 300 mm diameter at a speed of 20 mm s^{-1} with a thickness reduction of about 15% per pass to reduce the thickness to 4 mm, followed by air cooling. After each pass, the specimen was reheated to 1280 °C and soaked for 30 minutes. After rolling, a specimen was cut from the rolled sheet and was heat treated at 1250 °C for 1 hour followed by furnace cooling. The oxygen content and density for the as-cast, as-rolled and rolled + heat-treated samples were measured using the ELTRA ONH-2000 oxygen/nitrogen/hydrogen analyser and Micromeritics AccuPyc II 1340 Gas Pycnometer, respectively. The structural phase evolution in the rolled specimens was analysed by employing the X-ray diffraction (XRD) technique using the parameters Cu Kα radiation λ = 1.54062 Å and 2θ from 20° to 90° **[28**,**29]** with scan step size and speed of 0.02° and 0.002°/min respectively**.** The sample preparation procedure for the XRD examination outlined in **[29]** was adopted in this study. The microstructures of the as-cast, as-rolled and rolled + heat treated specimens were characterised by a JEOL JSM-6510 scanning electron microscope (SEM) in a

backscattered electron (BSE) mode. The obtained SEM-BSE images were used to determine the average grain sizes by utilizing the line intercept method in ImageJ software. Moreover, both the as-rolled and rolled + heat treated samples were also characterised by SEM electron backscattered diffraction (EBSD) technique and the gathered data were processed with Aztec ICE and HKL Channel 5 software. The EBSD parameters used were as follows; (a) acceleration voltage: 20 kV, (b) scanning interval: 0.4 μm and, (c) specimen tilted angle: 70° as reported in **[30]**. The specimens for SEM-BSE characterisation were prepared by grinding the specimen surfaces to a mirror-like finish using grit papers up to 1200 followed by 1 μm alumina, colloidal silica and then etched in 24 ml H_2O + 50 ml glycerol + 24 ml HNO_3 + 2 ml HF solution **[30]** while the ones for EBSD analysis were electro-polished in a solution of 600 ml methanol, 360 ml butoxyethanol and 60 ml perchloric acid after polishing mechanically up-to colloidal silica **[30]**. Micro Vickers hardness measurements were performed on the as-cast, as-rolled, and rolled + heat-treated specimens to obtain their hardness values. The specimens were prepared according to ASTM standard E3-11. This involved grinding and polishing the samples up to 1 μm diamond suspension. For hardness tests, a load of 500 gf was applied, and a dwelling time of 10 s was utilized as required by ASTM standards E384–05a **[35]**. The hardness values were given as averages of at-least 10 measurements taken at 0.5 mm intervals. To obtain mechanical properties viz. yield stresses, ultimate tensile stresses and strains of the specimens, a profilometry-based indentation plastometry (PIP) was employed. This equipment is utilised to obtain the best fit set of parameter values in a constitutive stress-strain law using the residual indent profile as the target outcome in a repeated finite element method (FEM) simulation **[36]**. It is noteworthy that this method of measuring tensile properties was found to agree well with the conventional tensile testing by Campbell et al. **[36]**. Specimen preparation for the tests was carried out by mounting and polishing to 1 μm finish **[36]**. The samples were then set on the plinth of the plastometer. The WC-Co cemented carbide spherical indenter of radius 1 mm was utilised to produce the indent using a force of 4.5 kN. During the testing, the average property values of six specimens for each alloy processing condition to ensure repeatability with three indentations on each specimen were obtained and recorded.

3. Results

3.1. X-ray diffraction (XRD) analysis

The structural transformation in the as-cast condition for this γ-TiAl-based alloy was reported by Mathabathe et al. **[31]**. The retained β-phase in addition to the ordered tetragonal γ-TiAl and close-packed hexagonal α_2-Ti_3Al phases as well as the titanium silicate (Ti_5Si_3) was obtained. **Fig. 1** shows the phases after hot-rolling and heat treatment. The major phases such as the tetragonal γ-TiAl (L_{10}), hexagonal α_2-Ti_3Al (DO_{19}), and titanium silicate (Ti_5Si_3) **[30]** were formed. Nevertheless, no retained β-phase is visible for both alloy conditions. It is noteworthy that the hexagonal α_2-Ti_3Al (DO_{19}) was categorised into α_2-(Ti_3Al) and α_2-(Alpha 2) depending on the slight difference in their crystal lattice parameters as shown in **Table 2**. The phases displayed the lattice parameters *a* and *b* to be equal to 5.72 Å for the former and 5.73 Å for the latter as also published in **[30]**. Moreover, the XRD peaks remained unchanged after heat-treatment of the hot rolled sample A. However, peak broadening was observed for the as-rolled material. This may be ascribed to the combined effects of the retained lattice strain after hot rolling as well as crystallite size as observed by Van Berkum et al., **[37].** To confirm the crystallite size and the accumulation of lattice strain in the as-rolled specimen, the Williamson-Hall (W-H) method was employed to analyse the XRD diffraction patterns **[38]**. The peaks' full-width-half maximum (FWHM) values were utilised to attain the W-H plots displayed in **Fig. 2a**,**b** for the as-rolled and rolled + heat treated, respectively. The slope values of the outstanding fit linear regression in the plots which represent the lattice strains of the systems are summarised in **Table 1** together with the crystallite sizes obtained using the y-intercepts of the plots **[39**–**41]**.

Table 1: The W-H crystallite size and lattice strains of the as-rolled and rolled + heat treated.

Table 2: Phase acquisition **[30]**

It is shown in **Fig. 2a** and **Table 1** that the slope of the plot is positive with a value of about 0.2183, and the average crystallite size is as small as 1.2926 nm for the as-rolled. This demonstrates that the crystallite sizes and the micro-strain in the as-rolled sample could be the main sources of peak broadening **[37,42]** observed in **Fig. 1**. Conversely, the negative slope displayed in **Fig. 2b** for the rolled + heat-treated sample shows that the effect of the micro-strain on the peak broadening was negligible **[38**,**43]**. However, as observed, the line plot is nearly flat and straight demonstrating a near-pure size broadening **[44]**.

Fig. 1: XRD phase identification of as-rolled (sample A) and rolled + heat-treated (sample B).

Fig. 2: The W-H plots for the (a) as-rolled (sample A), and (b) rolled + heat-treated (sample B).

3.2. Microstructures

Fig. 3 shows the microstructure of the (a,b) as-cast (c,d) as-rolled and (e,f) rolled + heat-treated alloy conditions. In the as-cast condition at lower magnification (a), the sample exhibits dendritic structures as previously observed **[31**,**45]**. However, at higher magnification (b), the α_2-Ti_3Al and γ-TiAl lamellae can be distinctly observed. In addition, due to the presence of Si, Ti has combined with Si to form clusters of titanium silicates (Ti_5Si_3) in the inter-dendritic region during solidification as illustrated in **Fig.3b**. Bibhanshu and Suwas **[46]** reported that the inter-dendritic regions of the solidified γ-TiAl-based cast alloy are consisting of γ-phase. **Fig. 3c,d** shows the initial coarse cellular-like dendritic structures observed in the as-cast microstructure (**Fig. 3a**) but consumed to form the typical "duplex" microstructural features far more uniform and refined with an mean grain size of about 3 μm. The microstructure consists of γ-phase, lamellar colonies of γ and α_2-phases, as well as a small amount of titanium silicate (Ti_5Si_3) precipitates. Due to the final rolling pass and subsequent air cooling, the grains are slightly elongated along the rolling direction as shown in **Fig. 3c**. This implies that the microstructure might still contain some micro-strain as evidenced by the diffraction peak broadening of the as-rolled specimen observed in **Fig. 1**. In **Fig. 3e,f** the microstructure of the hot rolled and heat treated alloy at 1250 °C for 1 hour is shown. The equiaxed grains emerged while the elongated grains disappeared in the as-rolled microstructure. This behaviour is attributed to the annihilation of micro-strain occured during heat treatment in agreement with the sharper diffraction XRD peaks (**Fig. 1)**.

Fig. 3: SEM-BSE micrographs, (LHS) low magnification and (RHS) high magnification (a) and (b) as-cast, (c) and (d) as-rolled sheet, (e) and (f) rolled + heat treated at 1250 °C for 1 hour.

3.3. SEM-EBSD analysis of microstructure

The as-rolled and rolled + heat-treated microstructures were further analysed by EBSD to gain insight into their phase transformation mechanisms. **Fig. 4a,b** display the EBSD layered images of the as-rolled and rolled + heat-treated specimens, respectively, at high magnification. In the as-rolled condition, the grain boundaries represented by a grey colour are broad. This behaviour might have occurred due to the remnant dislocation pile-up along the grain boundaries that were accumulated during the final rolling pass, validating the SEM-BSE and XRD results. Moreover, some of the α_2 and Ti_5Si_3-phases are dispersed in the γ-phase and along the γ/γ interfaces.

Fig.4: EBSD layered images (a) as-rolled, (b) rolled + heat-treated specimens.

Fig. 4b shows shows that the grain boundary broadening was dramatically reduced after heat treatment. Furthermore, the majority of the titanium silicate precipitates are situated along the grain boundaries. **Fig. 5** shows the EBSD map of the rolled + heat-treated specimen in which (a) is a band contrast, (b) phase maps, (c) orientation maps indicating inverse pole figures (IPF) in X, and (d) index maps with phase fractions in percentages. The dominating phase is the γ-phase **[30]** with the uppermost phase fraction of 86.5%. The α_2-phase (alpha 2 + alpha 2(Ti_3Al)) fraction is 5.68% while the Ti_5Si_3-phase fraction is 1.15%.

Fig. 5: EBSD map of the rolled + heat treated sample: a) band contrast, b) phase map, c) orientation map indicating inverse pole figure (IPF) in X, and d) index maps.

The boundary misorientation angles for α_2-(Ti_3Al), α_2-(alpha 2) and γ-(TiAl) in the rolled + heat-treated alloy condition are exhibited in **Fig. 6a-c**, respectively. It is apparent that for both α_2-Ti_3Al (**Fig. 6**a) and α_2-(alpha 2) (**Fig. 6b**) phases, the distributions show a large

number of boundaries with misorientations greater than 15° while for the γ-phase (**Fig. 6**c), the distribution exhibits almost all the misorientation angles greater than 15°.

Fig.6: Misorientation angle distribution of the rolled + heat-treated specimen (a) α_2-(Ti_3Al), (b) α_2-(alpha 2), (c) γ-(TiAl) phases, and (d) grain boundaries.

Fig.6d shows that a large percentage (99.7%) of grain boundaries in the alloy were misoriented at angles greater than 15°. The equivalent circle diameter grain size distribution in the rolled + heat-treated sheet is depicted in **Fig. 7**. It is evident that the microstructure mostly consisted of grains ranging from about 2 to 6 μm with a mean grain size of about 4μm.

Fig. 7: Histogram of equivalent circle diameter grain size distribution of the rolled and heat-treated alloy.

The microstructural texture representations of the rolled + heat-treated alloy are shown in **Fig. 8** in terms of pole figures and **Fig. 9** for the corresponding orientation distribution function (ODF) sections. The pole figures illustrate clusters on planes {100}, {110} and {111} for the existing phases in the sheet viz. α_2-Ti_3Al (**Fig. 8a**), α_2 (alpha 2) (**Fig. 8b**), γ-TiAl (**Fig. 8c**) and Ti_5Si_3 (**Fig. 8d**). Iin **Fig. 9** that the maximum intensity is observed at ϕ_2 = 30°, 35°, 40° and 45°. The predominant texture component resemble the familiar deformation and recrystallisation textures of face-centred cubic (FCC) metals **[24]** denoted by several researchers as a modified cube texture **[24**,**25].**

Fig. 8: Pole figures of {100}, {110} and {111} planes for (a) α_2-Ti_3Al, (b) α_2, (c) γ-TiAl, and (d) Ti_5Si_3 phases of the rolled + heat treated sheet.

Fig. 9: The orientation distribution function (ODF) sections of the rolled +heat-treated sheet.

3.4. Mechanical properties

Fig. 10 displays the mechanical properties in as-cast, as-rolled and rolled + heat-treated conditions. The relationship between the Vickers micro-hardness and the corresponding Image J and EBSD measured grain sizes of the alloy condition is shown in **Fig. 10a**. The as-rolled specimen possesses the highest hardness value of about 490 HV followed by the hot rolled and heat-treated sample with 398 HV. The lowest hardness value of 362 HV belongs to the as-cast sample. Upon heat treatment, the hardness dramatically dropped from 490 HV to 398 HV with a slight grain growth from the mean grain size of about 3 to 4 μm. The recorded tensile properties for as-cast, as-rolled and rolled + heat-treated specimens are illustrated in **Fig. 10b**. The rolled + heat-treated sample exhibits the balanced tensile properties with a yield stress of 528 MPa, the ultimate tensile stress of 796 MPa and a uniform elongation of 2.15%. On the contrary, the ductility of the as-rolled specimen deteriorated as evidenced by the lowest strain of 1.1%. This confirms that the material work-hardened and became brittle after hot-rolling and subsequent air cooling.

Fig. 10: Mechanical properties (a) micro-hardness and grain size, and (b) PIP estimation of the tensile properties under different processing conditions.

4. Discussion

4.1. Grain refinement mechanisms during hot-rolling and rapid cooling

Based on the experimental results, it is apparent that in this study a significant grain refinement was achieved primarily through hot rolling and subsequent rapid cooling. Prior to these processes, the as-cast microstructure consisted of dendrites (**Fig. 3a)** which usually form under non-equilibrium conditions. For this alloy system, Nb and Cr solutes tend to micro-segregate to the cores of solidifying dendrites during the solidification process. As Ti, Nb and Cr segregate to the emerging dendrites, the Al diffuses to the inter-dendritic regions **[31**,**47]**. Consequently, the cast microstructure becomes inhomogeneous and thus negatively affects its hot workability **[48**,**49]**. However, a homogenization treatment was carried out at every rolling stage as elucidated in section 2 to minimize chemical segregation and hence mitigate detrimental microstructural inhomogeneity **[50]**. During hot-rolling, plastic stresses activate the movement of dislocations in a material. As more lattice dislocations are absorbed by the subgrain boundaries, the increase in misorientation of the boundaries occurs, and gradually the boundaries transform into high-angle grain boundaries (HAGBs) **[51]**. This development of HAGBs eliminates the subgrain and original grain boundaries and new equiaxed grains emerge through the process of continuous recrystallization **[52**–**54]**. When the sample experienced air rapidly cooling after the final rolling pass from just below the α-transus (α+γ region) temperature, the γ-grains and Ti_5Si_3 precipitated and nucleated during rolling, was suppressed due to the inadequate diffusion time. Furthermore, owing to the rolling deformation, there was micro-strain retention as exhibited by the positive slope of the plot in **Fig. 2a** and the elongation of the grains along the rolling direction in **Fig. 3c**. This behaviour might have affected the transformation of α to $\alpha_2 + \gamma$ ($\alpha \rightarrow \alpha_2 + \gamma$) in a similar way to strain-induced transformation **[55**,**56]** in which a combination of high strain and undercooling becomes the driving force for transformation. It required a 1h heat treatment time to annihilate the micro-strain in the material and reactivate the diffusion mechanisms

to produce a more equiaxed grains illustrated in **Fig. 3e**. Moreover, the microstructure appears to contain twin boundaries (TBs) as depicted in **Fig. 3f**. As explained by Mandal et al.,**[57]** the TBs are expected in the dynamic recrystallised (DRX) grains. These TBs are formed by "growth accidents" during the expansion of the recrystallised grains. This phenomenon takes place when the stored energy is exhausted and wen the orientation between the recrystallized and deformed grains is similar **[54].** The confirmation for the occurrence of DRX during hot-rolling is provided in **Fig. 6d** which illustrates that the predominant type of grain boundary in the sheet after rolling and subsequent heat treatment was the high-angle grain boundary (HAGB) **[53]** which is generally suggested to be caused by DRX **[25]**.

4.2. Texture evolution of the rolled and heat-treated sheet

The texture development in γ-TiAl-based alloys during hot rolling has been studied by several researchers for alloys containing both less and high Nb **[25**,**58**–**61]**. The studies have concluded that the main texture component in both categories of alloy is a modified cube texture in which the [001] in the γ-phase align along the sheet's transverse direction during hot-rolling with subsequent recrystallization of γ-TiAl alloys. However, the orientation density in the sheets varies from one alloy system to another depending on the content of Nb. For those in the conventional γ-TiAl alloy with low content of Nb, the texture is much strong, while those containing high Nb have a considerably weak texture. Concerning the high Nb γ-TiAl alloys, Shen et al., **[25]** published a maximum orientation density of three times denser than a random distribution for a Ti-45Al-8.5Nb-(W, B, Y) (at.%) sheet that was directly hot-pack rolled from an ingot prepared using plasma arc melting (PAM) process. For the low Nb alloys, Bartels and Schillinger **[58]** investigated the hot-rolling texture evolution of a rolled Ti-46.5Al-4(Cr, Nb, Ta, B) (at. %) alloy prepared by powder metallurgy. They found that the maximum orientation density was five times higher than the random. In another study, Bartels et al., **[59]** reported the orientation density of a Ti-47Al-4(Cr, Mn, Nb, Si, B) sheet that was rolled and primary annealed for two hours at 1000 °C to be twelve times stronger than the random. On the contrary, it has been shown in the current study that the orientation density in the sheet (low Nb-

containing alloy) is only about 2.4 times stronger than a random distribution (**Fig. 9**). Therefore, a weak anisotropy of mechanical properties in the material is expecyted. This less orientation density can be attributed to the beneficial results of suppressing the growth of recrystallized grains.

4.3. Analysis of mechanical properties

The properties such as hardness, strength and ductility in γ-TiAl-based alloys are related to the grain size. Generally, fine grains result in high hardness and strength **[28**,**62]**. This behaviour is best elucidated with the well-known Hall-Petch relationship shown in equation (1) **[28]**.

$$\sigma_Y = \sigma_0 + Kd^{-1/2}. \quad (1)$$

σ_Y is yield strength for permanent deformation of the material, σ_0 and K are constants for the alloy and d is the mean diameter of the grains. For the as-rolled specimen, the fast cooling of the sample in the air after hot rolling prevented the growth of recrystallized grains and resulted in the production of fine grains in the microstructure with a mean grain size of about 3 μm as shown in **Fig. 10a**. These fine grains may be a reason for high hardness value of 490 HV **[63]**. However, as noticed from the XRD and EBSD results (**Fig. 1** and **Fig. 4**a), this samples contained a micro-strain which accumulated during the final rolling pass. The work hardening also contributed to the final hardness value of the sample. After heat treating the rolled sample, the hardness dropped to 398 HV with an almost negligible grain growth. This may further confirm the presence of micro-strain in the as-rolled sample which was annihilated during heat treatment. As shown in section 3.2, the microstructure of the as-cast consist of coarse lamellar colonies with ultrafine lamellar spacing as exhibited in **Fig. 3b**. In this case, Dimiduk et al., **[64]** concluded that for polycrystalline lamellar alloys, the lamellar interfaces become the dominant barriers for dislocation glide and thus play a key role in influencing strength as well as hardness. On the other hand, the microstructure of the specimen rolled and heat-treated is duplex (**Fig. 3e)** of which its mechanical properties are controlled by both the phases of the

microstructure and the grain size **[65]**. Furthermore, in **Fig. 10b**, the specimen that was rolled and heat-treated displays balanced mechanical properties attributable to the homogeneous and relaxed microstructure. It is also evident that the values of mechanical properties obtained from this study viz. 398HV, 528 MPa, 796 MPa and 2.15% for the hardness, yield stress, ultimate tensile strength and elongation respectively, thus the rolled and heat-treated sample is superior to the data reported in literature for similar hot-rolled peritectic-solidifying (i.e. L + $\beta \rightarrow \alpha$) low Nb containing γ-TiAl based sheets **[27]**.

5. Conclusion

The combined effects of hot-rolling, rapid cooling, and heat treatment on the grain refinement of a γ-TiAl-based sheet of nominal composition Ti-48Al-2Nb-0.7Cr-0.3Si were investigated in this study. The main aim was to cost-effectively improve the mechanical properties of the sheet by further refining its grain size. From the obtained results, the following conclusions were drawn:

- A 13 mm thick as-cast ingot produced by VAR was successfully hot-pack rolled in the $\alpha+\gamma$ region to a thickness of 4 mm using a conventional two-high rolling mill followed by air cooling after the final pass.
- A slightly elongated, equiaxed and fine DRX microstructure of a mean grain size of about 3 μm was produced after air cooling. The microstructure mainly consisted of γ-phase, $\gamma+\alpha_2$ lamellar colonies and precipitates of Ti_5Si_3 predominantly situated along the grain boundaries. The dynamically recrystallized grains slightly grew to an average grain size of about 4 μm, and became more equiaxed and homogeneous when heat treatment was performed on the rolled sheet.
- The EBSD texture analysis illustrated that the micro-texture of the resulting sheet was the cube texture with an orientation density of about two times the random orientation distributions.
- The mechanical properties of the rolled+heat-treated specimen were balanced and improved compared to the ones of the as-cast and as-rolled samples. In

general, it can be inferred that a hot-rolling process can be employed together with rapid cooling and heat treatment to obtain a more refined and homogeneous microstructure. However, precautions must be taken to ensure that all the process parameters are precisely controlled to avoid deterioration of the resulting mechanical properties.

Acknowledgements

The authors would like to acknowledge the Council of Scientific and Industrial Research for funding this work, the University of Pretoria and Mintek for the provision of the laboratory equipment. Many thanks should also go to Mr Carel Coetzee and Mr Christiaan C. E. Pretorius for the technical support.

References

[1] W. Smarsly, H. Baur, G. Glitz, H. Clemens, T. Khan, and M. Thomas, “Titanium aluminides for automotive and gas turbine application, in: K.J. Hemker, et al. (Ed.), Structural Intermetallics 2001,” in *The Minerals, Metals and Materials Society (TMS)*, 2001, pp. 25–34.

[2] M. J. Weimer, B. Bewlay, and T. Schubert, “GEnx TiAl LPT blade status and lean flow casting at GE Aviation Deutschland, Presentation at 4th International Workshop on Titanium Aluminides,” 2011.

[3] H. Clemens and S. Mayer, “Design, processing, microstructure, properties, and applications of advanced intermetallic TiAl alloys,” *Adv. Eng. Mater.*, vol. 15, no. 4, pp. 191–215, 2013, doi: 10.1002/adem.201200231.

[4] H. Clemens, W. Wallgram, S. Kremmer, V. Güther, A. Otto, and A. Bartels, “Design of novel β-solidifying TiAl alloys with adjustable β/B2-phase fraction and excellent hot-workability,” *Adv. Eng. Mater.*, vol. 10, no. 8, pp. 707–713, 2008, doi: 10.1002/adem.200800164.

[5] S. Bolz *et al.*, “Microstructure and mechanical properties of a forged β-solidifying γ TiAl alloy in different heat treatment conditions,” *Intermetallics*, vol. 58, pp. 71–83, 2015, doi: 10.1016/j.intermet.2014.11.008.

[6] W. E. Voice, M. Henderson, E. F. J. Shelton, and X. Wu, “Gamma titanium aluminide, TNB,” *Intermetallics*, vol. 13, no. 9, pp. 959–964, 2005, doi: 10.1016/j.intermet.2004.12.021.

[7] E. Schwaighofer *et al.*, “Microstructural design and mechanical properties of a cast and heat-treated intermetallic multi-phase γ-TiAl based alloy,” *Intermetallics*, vol. 44, pp. 128–140, 2014, doi: 10.1016/j.intermet.2013.09.010.

[8] Y. W. (Y W.). Kim, “Microstructural evolution and mechanical properties of a forged gamma titanium aluminide alloy,” *Acta Metall. Mater.*, vol. 40, no. 6, pp. 1121–1134, 1992, doi: 10.1016/0956-7151(92)90411-7.

[9] Y. W. Kim, “Ordered intermetallic alloys, part III: Gamma titanium aluminides,” *Jom*, vol. 46, no. 7, pp. 30–39, 1994, doi: 10.1007/BF03220745.

[10] M. Oehring, A. Stark, J. D. H. Paul, T. Lippmann, and F. Pyczak, “Microstructural refinement of boron-containing β-solidifying γ-titanium aluminide alloys through heat treatments in the β phase field,” *Intermetallics*, vol. 32, pp. 12–20, 2013, doi: 10.1016/j.intermet.2012.08.010.

[11] L. DE, C. L, K. SL, and S. P, “DEFORMATION OF TIB2-REINFORCED NEAR-GAMMA TITANIUM ALUMINIDES,” *Mater Sci Eng*, vol. A144, pp. 45–49, 1999.

[12] T. T. Cheng, “Mechanism of grain refinement in TiAl alloys by boron addition - an alternative hypothesis,” *Intermetallics*, vol. 8, no. 1, pp. 29–37, 2000, doi: 10.1016/S0966-9795(99)00063-1.

[13] D. Hu, “Effect of composition on grain refinement in TiAl-based alloys,” *Intermetallics*, vol. 9, no. 12, pp. 1037–1043, 2001, doi: 10.1016/S0966-9795(01)00079-6.

[14] J. Li, S. Jeffs, M. Whittaker, and N. Martin, “Boride formation behaviour and their effect on tensile ductility in cast TiAl-based alloys,” *Mater. Des.*, vol. 195, p. 109064, 2020, doi: 10.1016/j.matdes.2020.109064.

[15] J. N. Wang and K. Xie, “Grain size refinement of a TiAl alloy by rapid heat treatment,” *Scr. Mater.*, vol. 43, no. 5, pp. 441–446, 2000, doi: 10.1016/S1359-6462(00)00419-X.

[16] J. N. Wang, J. Yang, and Y. Wang, “Grain refinement of a Ti-47Al-8Nb-2Cr alloy through heat treatments,” *Scr. Mater.*, vol. 52, no. 4, pp. 329–334, 2005, doi: 10.1016/j.scriptamat.2004.10.004.

[17] J. Yang, J. N. Wang, Y. Wang, Q. Xia, and B. Zhang, “Control of the homogeneity of the lamellar structure of a TiAl alloy refined by heat treatment,” *Intermetallics*, vol. 9, no. 5, pp. 369–372, 2001, doi: 10.1016/S0966-9795(01)00020-6.

[18] V. M. Imayev, R. M. Imayev, and T. G. Khismatullin, “Mechanical properties of the cast intermetallic alloy Ti-43Al-7(Nb,Mo)-0.2B (at %) after heat treatment,” *Phys. Met. Metallogr.*, vol. 105, no. 5, pp. 484–490, 2008, doi: 10.1134/S0031918X08050098.

[19] B. Tang, L. Cheng, H. Kou, and J. Li, “Hot forging design and microstructure evolution of a high Nb containing TiAl alloy,” *Intermetallics*, vol. 58, no. March, pp. 7–14, 2015, doi: 10.1016/j.intermet.2014.11.002.

[20] A. Bartels, C. Koeppe, and H. Mecking, “Microstructure and properties of Ti-48Al-2Cr after thermomechanical treatment,” *Mater. Sci. Eng. A*, vol. 192–193, no. PART 1, pp. 226–232, 1995, doi: 10.1016/0921-5093(94)03251-3.

[21] M. Burtscher *et al.*, “An advanced tial alloy for high-performance racing applications,” *Materials (Basel).*, vol. 13, no. 21, pp. 1–14, 2020, doi: 10.3390/ma13214720.

[22] C. Hartig, X. F. Fang, H. Mecking, and M. Dahms, “Textures and plastic anisotropy in γ-TiAl,” *Acta Metall. Mater.*, vol. 40, no. 8, pp. 1883–1894, 1992, doi: 10.1016/0956-7151(92)90175-E.

[23] S. L. Semiatin, B. W. Shanahan, and F. Meisenkothen, “Hot rolling of gamma titanium aluminide foil,” *Acta Mater.*, vol. 58, no. 13, pp. 4446–4457, 2010, doi: 10.1016/j.actamat.2010.04.042.

[24] W. Schillinger, A. Bartels, R. Gerling, F. P. Schimansky, and H. Clemens, “Texture evolution of the γ- And the α/α 2-phase during hot rolling of γ-TiAl based alloys,” *Intermetallics*, vol. 14, no. 3, pp. 336–347, 2006, doi: 10.1016/j.intermet.2005.07.002.

[25] Z. Z. Shen, J. P. Lin, Y. F. Liang, L. Q. Zhang, S. L. Shang, and Z. K. Liu, “A novel hot pack rolling of high Nb-TiAl sheet from cast ingot,” *Intermetallics*, vol. 67, pp. 19–25, 2015, doi: 10.1016/j.intermet.2015.07.009.

[26] A. Ellard, J.J.M, Mathabathe, M.N, Siyasiya, C.W, Bolokang, “POWDER CHARACTERISTICS BLENDING AND MICROSTRUCTURAL ANALYSIS OF A HOT-PACK ROLLED VACUUM ARC-MELTED GAMMA-TIAL-BASED SHEET,” *SAJIE*, vol. 33, no. 3, pp. 274–283, 2022.

[27] H. Clemens, I. Rumberg, P. Schretter, and S. Schwantes, “Characterization of Ti48Al2Cr sheet material,” *Intermetallics*, vol. 2, no. 3, pp. 179–184, 1994, doi: 10.1016/0966-9795(94)90056-6.

[28] M. N. Mathabathe, A. S. Bolokang, G. Govender, R. J. Mostert, and C. W. Siyasiya, “The vacuum melted ɣ-TiAl (Nb, Cr, Si)-doped alloys and their cyclic oxidation properties,” *Vacuum*, vol. 154, no. May, pp. 82–89, 2018, doi: 10.1016/j.vacuum.2018.04.055.

[29] M. N. Mathabathe, A. S. Bolokang, G. Govender, C. W. Siyasiya, and R. J. Mostert, “Cold-pressing and vacuum arc melting of γ-TiAl based alloys,” *Adv. Powder Technol.*, vol. 30, no. 12, pp. 2925–2939, 2019, doi: 10.1016/j.apt.2019.08.038.

[30] M. N. Mathabathe, A. S. Bolokang, G. Govender, R. J. Mostert, and C. W. Siyasiya, “Structure-property orientation relationship of a γ/α2/Ti5Si3 in as-cast Ti-45Al-2Nb-0.7Cr-0.3Si intermetallic alloy,” *J. Alloys Compd.*, vol. 765, pp. 690–699, 2018, doi: 10.1016/j.jallcom.2018.06.265.

[31] M. N. Mathabathe, S. Govender, A. S. Bolokang, R. J. Mostert, and C. W. Siyasiya, “Phase transformation and microstructural control of the α-solidifying γ-Ti-45Al-2Nb-0.7Cr-0.3Si intermetallic alloy,” *J. Alloys Compd.*, vol. 757, pp. 8–15, 2018, doi: 10.1016/j.jallcom.2018.05.051.

[32] Z. Jun-hong, H. Bai-yun, and Z. Ke-chao, “Pack rolling of TieAl based alloy.,” *Chinese J. Nonferrous Met.*, vol. 11, no. 6, pp. 1055–1058, 2001.

[33] L. Yong, H. Bai-yun, and Z. Ke-chao, “Canned forging process of TiAl based alloy,” *Chinese J. Nonferrous Met.*, vol. 10, no. 1, pp. 6–9, 2000.

[34] J. song Huang *et al.*, “Simulation of hot compression of Ti-Al alloy,” *Intermetallics*, vol. 15, no. 5–6, pp. 700–705, 2007, doi: 10.1016/j.intermet.2006.10.019.

[35] ASTM E384, “Standard Test Method for Microindentation Hardness of Materials ASTM E384,” *ASTM Stand.*, vol. 14, pp. 1–24, 2002.

[36] J. E. Campbell *et al.*, “A Critical Appraisal of the Instrumented Indentation Technique and Profilometry-Based Inverse Finite Element Method Indentation Plastometry for Obtaining Stress–Strain Curves,” *Adv. Eng. Mater.*, vol. 23, no. 5, 2021, doi: 10.1002/adem.202001496.

[37] J. G. M. van Berkum, A. C. Vermeulen, R. Delhez, T. H. de Keijser, and E. J. Mittemeijer, “Applicabilities of the Warren-Averbach analysis and an alternative analysis for separation of size and strain broadening,” *J. Appl. Crystallogr.*, vol. 27, no. pt 3, pp. 345–357, 1994, doi: 10.1107/S0021889893010568.

[38] A. S. Bolokang, M. N. Mathabathe, S. Chikosha, and D. E. Motaung, “Investigating the heat resistant properties of the TiNi shape memory alloy on the B19′→B2 phase transformation using the alloy powder,” *Surfaces and Interfaces*, vol. 20, no. July, p. 100608, 2020, doi: 10.1016/j.surfin.2020.100608.

[39] A. J. C. Langford, J. I., Wilson, “Scherrer after sixty years: A survey and some new results in the determination of crystallite size,” *J. Appl. Crystallogr.*, vol. 11, pp. 102–113, 1978.

[40] L. E. Klug, H.P., Alexander, *X-ray Diffraction procedures for Polycrystalline and Amorphous Materials*. New York: Wiley, 1974.

[41] S. Fatimah, R. Ragadhita, D. Fitria, A. Husaeni, A. Bayu, and D. Nandiyanto, “ASEAN Journal of Science and Engineering How to Calculate Crystallite Size from X-Ray Diffraction (XRD) using Scherrer Method,” *J. Sci. Eng.*, vol. 2, no. 1, pp. 65–76, 2022.

[42] D. Balzar, “X-ray diffraction line broadening: modeling and applications to high-Tc superconductors,” *J. Res. Natl. Inst. Stand. Technol.*, vol. 98, no. 3, p. 321, 1993, doi: 10.6028/jres.098.026.

[43] J. I. Langford, R. J. Cernik, and D. Louer, “Breadth and shape of instrumental line profiles in high-resolution powder diffraction,” *J. Appl. Crystallogr.*, vol. 24, no. pt 5, pp. 913–919, 1991, doi: 10.1107/S0021889891004375.

[44] K. R. Beyerlein, R. L. Snyder, M. Li, and P. Scardi, “Application of the Debye function to systems of crystallites,” *Philos. Mag.*, vol. 90, no. 29, pp. 3891–3905, 2010, doi: 10.1080/14786435.2010.501769.

[45] N. Bibhanshu, G. Shankar, and S. Suwas, “Hot deformation and softening response in boronmodified two-phase titanium aluminide Ti–48Al–2V–0.2B,” *J. Mater. Res.*, vol. 36, no. 1, pp. 311–321, 2021, doi: 10.1557/s43578-020-00079-0.

[46] N. Bibhanshu and S. Suwas, “Hot deformation and dynamic recrystallization in titanium aluminide,” *Mater. Sci. Forum*, vol. 941, no. December, pp. 1391–1396, 2018, doi: 10.4028/www.scientific.net/MSF.941.1391.

[47] X. F. Ding, J. P. Lin, L. Q. Zhang, H. L. Wang, G. J. Hao, and G. L. Chen, “Microstructure development during directional solidification of Ti-45Al-8Nb alloy,” *J. Alloys Compd.*, vol. 506, no. 1, pp. 115–119, 2010, doi: 10.1016/j.jallcom.2010.06.151.

[48] F. Appel *et al.*, “Recent progress in the development of gamma titanium aluminide alloys,” *Adv. Eng. Mater.*, vol. 2, no. 11, pp. 699–720, 2000, doi: 10.1002/1527-

2648(200011)2:11<699::AID-ADEM699>3.0.CO;2-J.

[49] S. L. Semiatin, G. R. Cornish, and D. Eylon, “Hot-compression behavior and microstructure evolution of pre-alloyed powder compacts of a near-γ titanium aluminide alloy,” *Mater. Sci. Eng. A*, vol. 185, no. 1–2, pp. 45–53, 1994, doi: 10.1016/0921-5093(94)90926-1.

[50] F. Appel, J. D. H. Paul, M. Oehring, and J. D. H. P. and M. O. Fritz Appel, *Gamma Titanium Aluminide Alloys*. 2011.

[51] Q. Wang, R. Zhou, Y. Li, and B. Geng, “Characteristics of dynamic recrystallization in semi-solid CuSn10P1 alloy during hot deformation,” *Mater. Charact.*, vol. 159, no. September 2019, p. 109996, 2020, doi: 10.1016/j.matchar.2019.109996.

[52] W. Zhang, Y. Liu, H. Z. Li, Z. Li, H. Wang, and B. Liu, “Journal of Materials Processing Technology Constitutive modeling and processing map for elevated temperature flow behaviors of a powder metallurgy titanium aluminide alloy,” vol. 209, pp. 5363–5370, 2009, doi: 10.1016/j.jmatprotec.2009.04.006.

[53] X. Chen *et al.*, “Dynamic recrystallization and hot processing map of Ti-48Al-2Cr-2Nb alloy during the hot deformation,” *Mater. Charact.*, vol. 179, no. 127, p. 111332, 2021, doi: 10.1016/j.matchar.2021.111332.

[54] X. T. Zhong, L. K. Huang, and F. Liu, “Discontinuous Dynamic Recrystallization Mechanism and Twinning Evolution during Hot Deformation of Incoloy 825,” *J. Mater. Eng. Perform.*, vol. 29, no. 9, pp. 6155–6169, 2020, doi: 10.1007/s11665-020-05093-1.

[55] M. R. Hickson, P. J. Hurley, R. K. Gibbs, G. L. Kelly, and P. D. Hodgson, “The production of ultrafine ferrite in low-carbon steel by strain-induced transformation,” *Metall. Mater. Trans. A Phys. Metall. Mater. Sci.*, vol. 33, no. 4, pp. 1019–1026, 2002, doi: 10.1007/s11661-002-0203-5.

[56] H. Dong and X. Sun, “Deformation induced ferrite transformation in low carbon steels,” *Curr. Opin. Solid State Mater. Sci.*, vol. 9, no. 6, pp. 269–276, 2005, doi: 10.1016/j.cossms.2006.02.014.

[57] S. Mandal, A. K. Bhaduri, and V. S. Sarma, “Role of twinning on dynamic recrystallization and microstructure during moderate to high strain rate hot deformation of a ti-modified austenitic stainless steel,” *Metall. Mater. Trans. A Phys. Metall. Mater. Sci.*, vol. 43, no. 6, pp. 2056–2068, 2012, doi: 10.1007/s11661-011-1012-5.

[58] A. Bartels and W. Schillinger, “Micromechanical mechanism of texture formation in γ-TiAl,” *Intermetallics*, vol. 9, no. 10–11, pp. 883–889, 2001, doi: 10.1016/S0966-9795(01)00086-3.

[59] A. Bartels, H. Kestler, and H. Clemens, “Deformation behaviour of differently

precessed γ-titanium aluminides," *Mater. Sci. Eng. A*, vol. 329–331, pp. 153–162, 2002, doi: 10.1016/S0921-5093(01)01552-0.

[60] A. Stark, A. Bartels, F. P. Schimansky, and H. Clemens, "Texture Formation in High Niobium Containing TiAl Alloys," *MRS Online Proc. Libr.*, vol. 980, no. 701, 2006, doi: 10.1557/PROC-980-0980-II07-01.

[61] A. Stark, A. Bartels, R. Gerling, F. P. Schimansky, and H. Clemens, "Microstructure and texture formation during hot rolling of niobium-rich γ TiAl alloys with different carbon contents," *Adv. Eng. Mater.*, vol. 8, no. 11, pp. 1101–1108, 2006, doi: 10.1002/adem.200600127.

[62] Y. W. Kim, "Strength and ductility in TiAl alloys," *Intermetallics*, vol. 6, no. 7–8, pp. 623–628, 1998, doi: 10.1016/s0966-9795(98)00037-5.

[63] Y. Bhambri, V. K. Sikka, W. D. Porter, E. A. Loria, and T. Carneiro, "Effect of composition and cooling rate on the transformation of α to γ phase in TiAl alloys," *Mater. Sci. Eng. A*, vol. 424, no. 1–2, pp. 361–365, 2006, doi: 10.1016/j.msea.2006.03.030.

[64] D. M. Dimiduk, P. M. Hazzledine, T. A. Parthasarathy, S. Seshagiri, and M. G. Mendiratta, "The role of grain size and selected microstructural parameters in strengthening fully lamellar TiAl alloys," *Metall. Mater. Trans. A Phys. Metall. Mater. Sci.*, vol. 29, no. 1, pp. 37–47, 1998, doi: 10.1007/s11661-998-0157-3.

[65] F. Appel, M. Oehring, and R. Wagner, "Novel design concepts for gamma-base titanium aluminide alloys," *Intermetallics*, vol. 8, no. 9–11, pp. 1283–1312, 2000, doi: 10.1016/S0966-9795(00)00036-4.

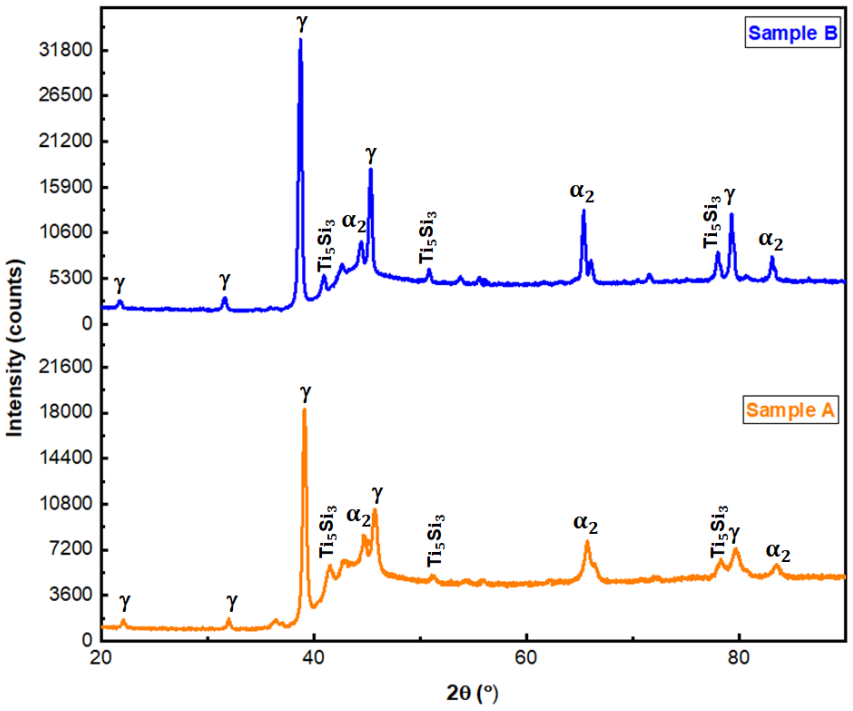

Fig. 1: XRD phase identification of as-rolled (sample A) and rolled + heat-treated (sample B).

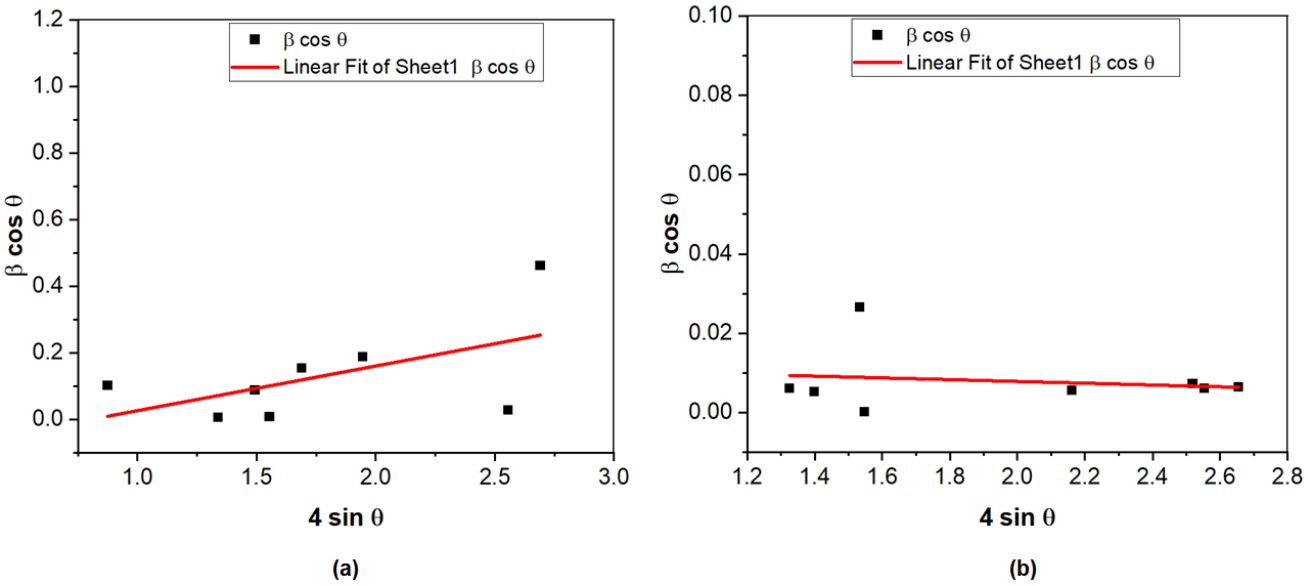

Fig. 2: The W-H plots for the (a) as-rolled (sample A), and (b) rolled + heat-treated (sample B).

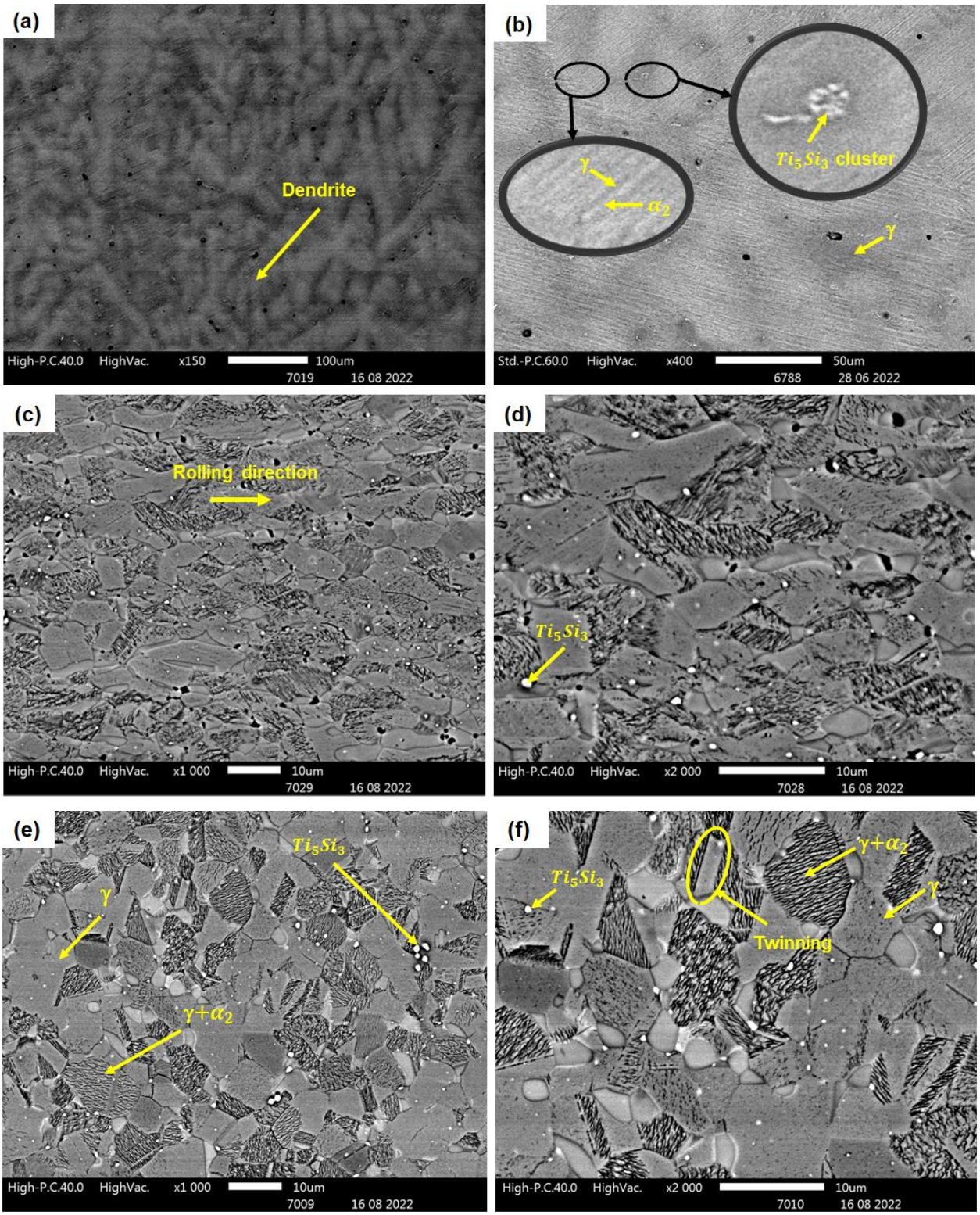

Fig. 3: SEM-BSE micrographs, (LHS) low magnification and (RHS) high magnification (a) and (b) as-cast, (c) and (d) as-rolled sheet, (e) and (f) rolled + heat treated at 1250 °C for 1 hour.

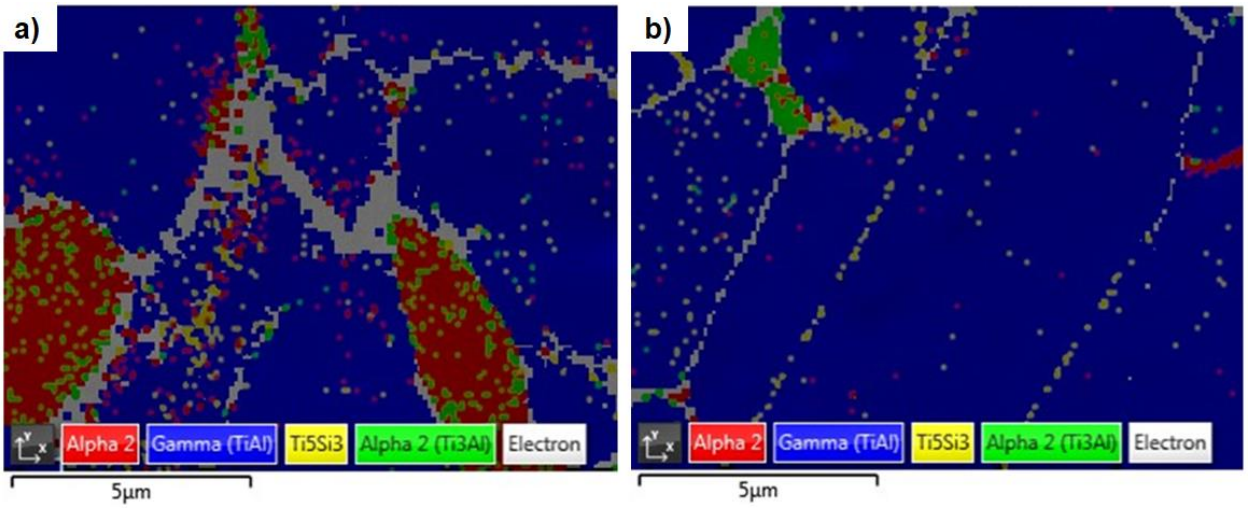

Fig.4: EBSD layered images (a) as-rolled, (b) rolled + heat-treated specimens.

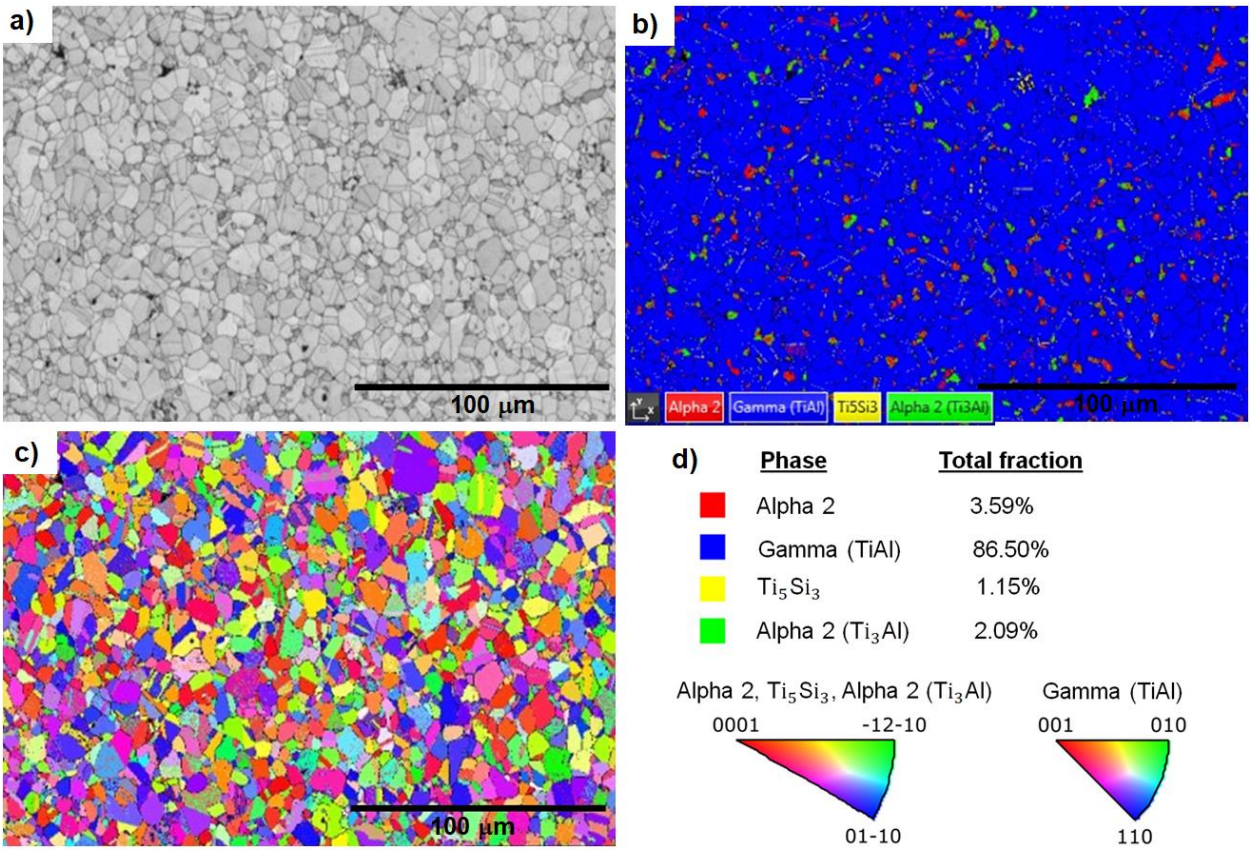

Fig. 5: EBSD map of the rolled + heat treated sample: a) band contrast, b) phase map, c) orientation map indicating inverse pole figure (IPF) in X, and d) index maps.

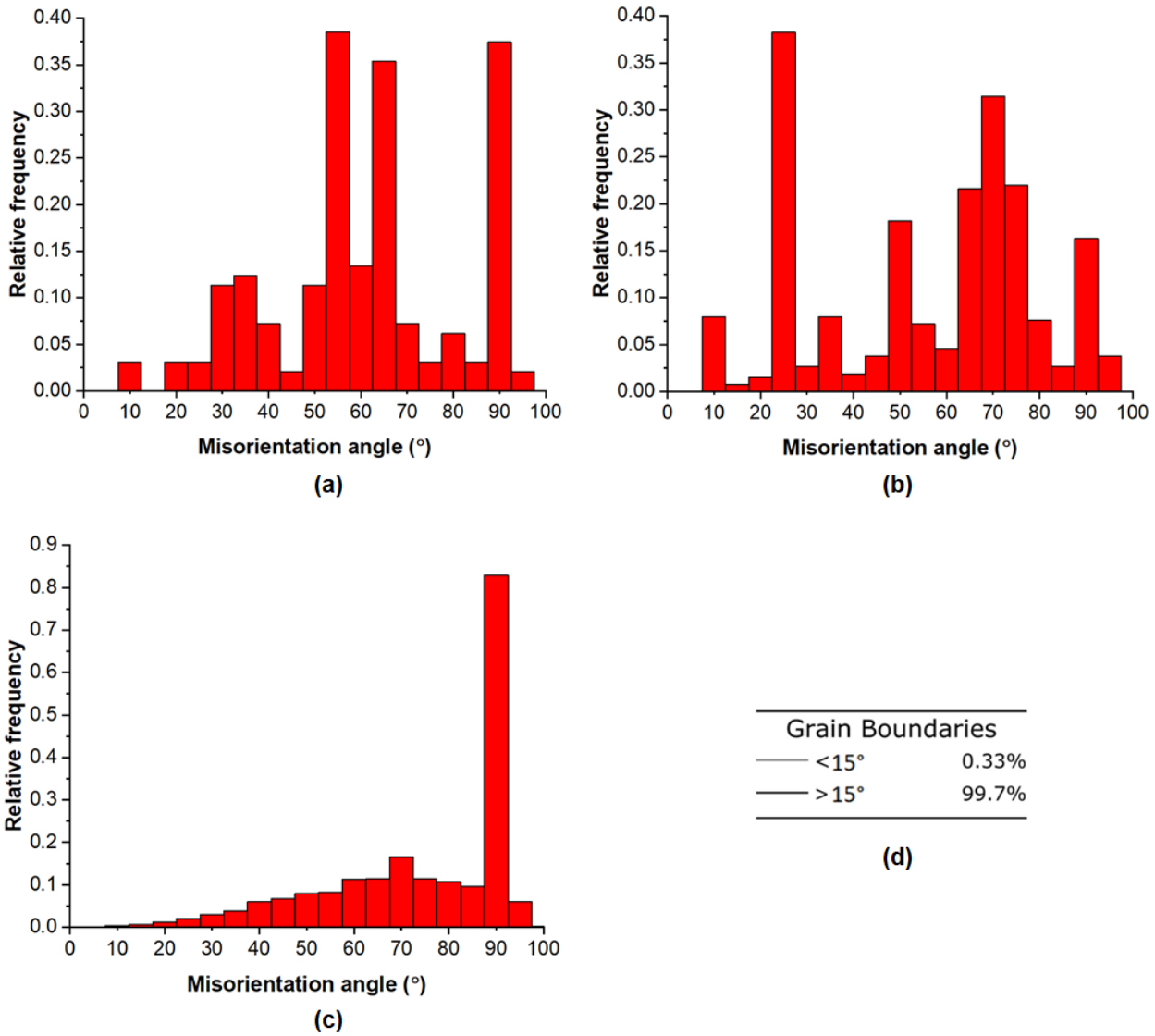

Fig.6: Misorientation angle distribution of the rolled + heat-treated specimen (a) α_2-(Ti_3Al), (b) α_2-(alpha 2), (c) γ-(TiAl) phases, and (d) grain boundaries.

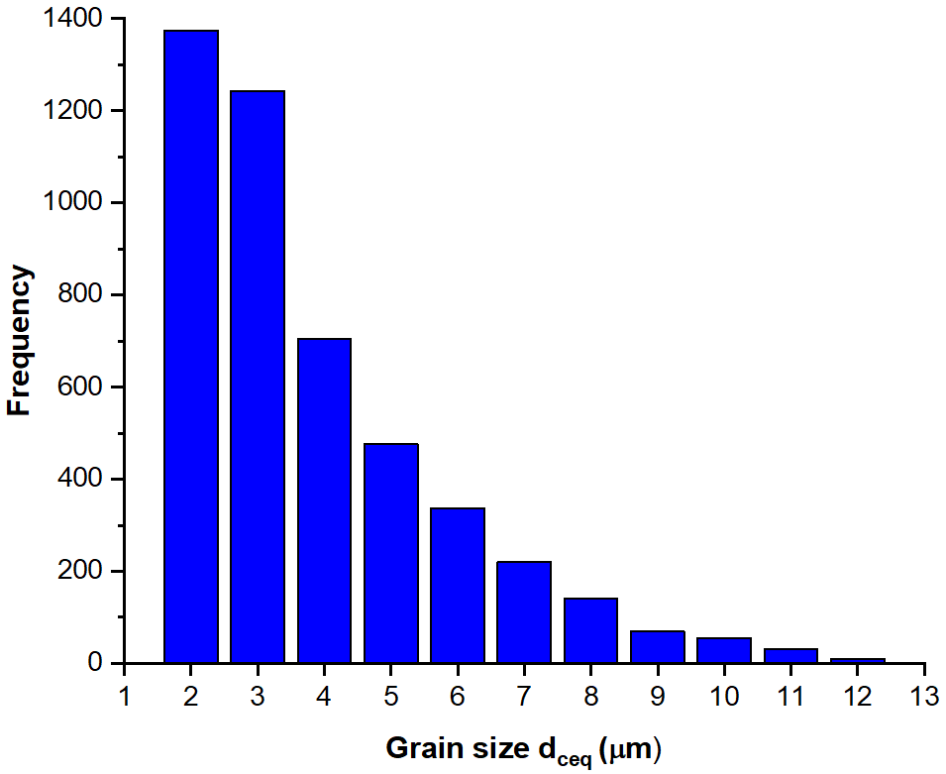

Fig. 7: Histogram of equivalent circle diameter grain size distribution of the rolled and heat-treated alloy.

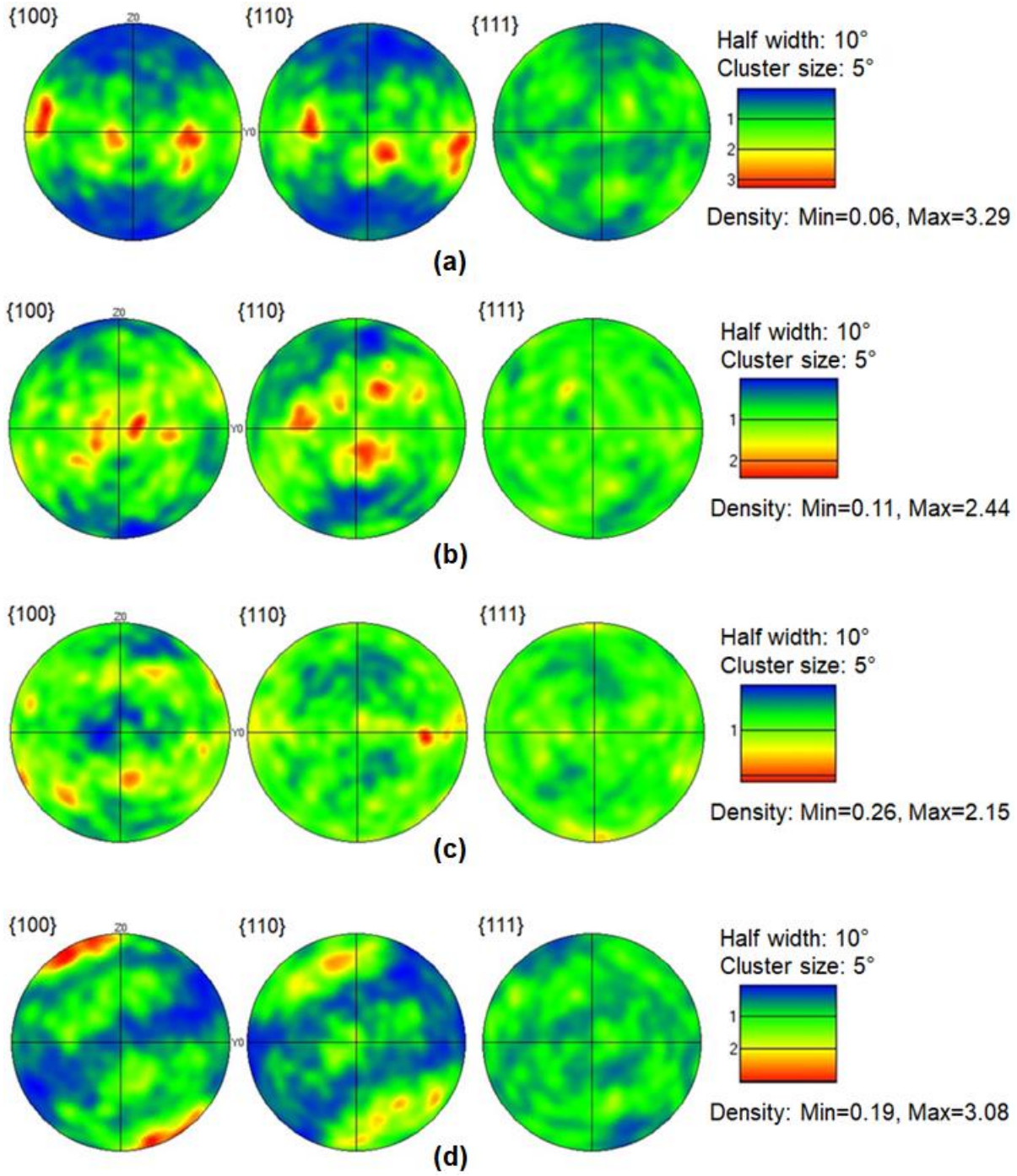

Fig. 8: Pole figures of {100}, {110} and {111} planes for (a) α_2-Ti_3Al, (b) α_2, (c) γ-TiAl, and (d) Ti_5Si_3 phases of the rolled + heat treated sheet.

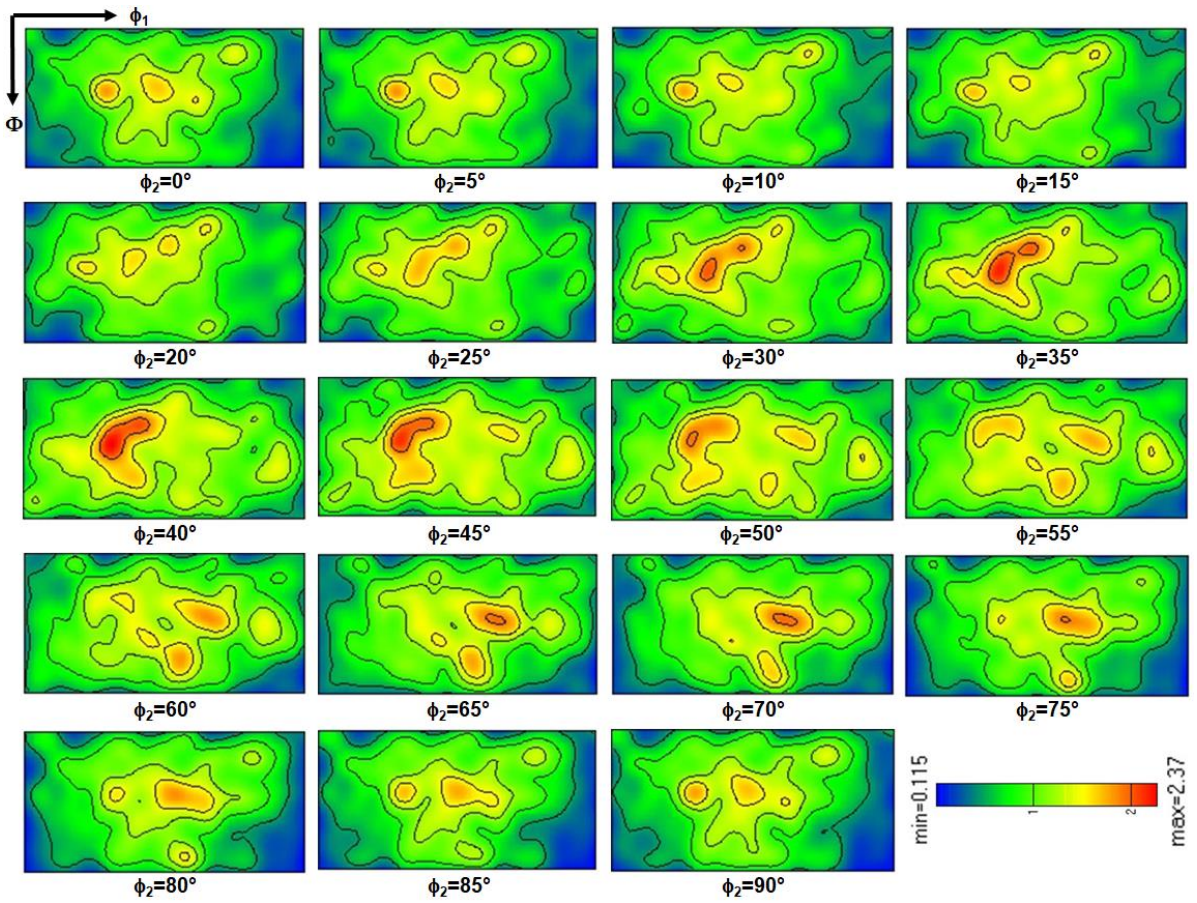

Fig. 9: The orientation distribution function (ODF) sections of the rolled +heat-treated sheet.

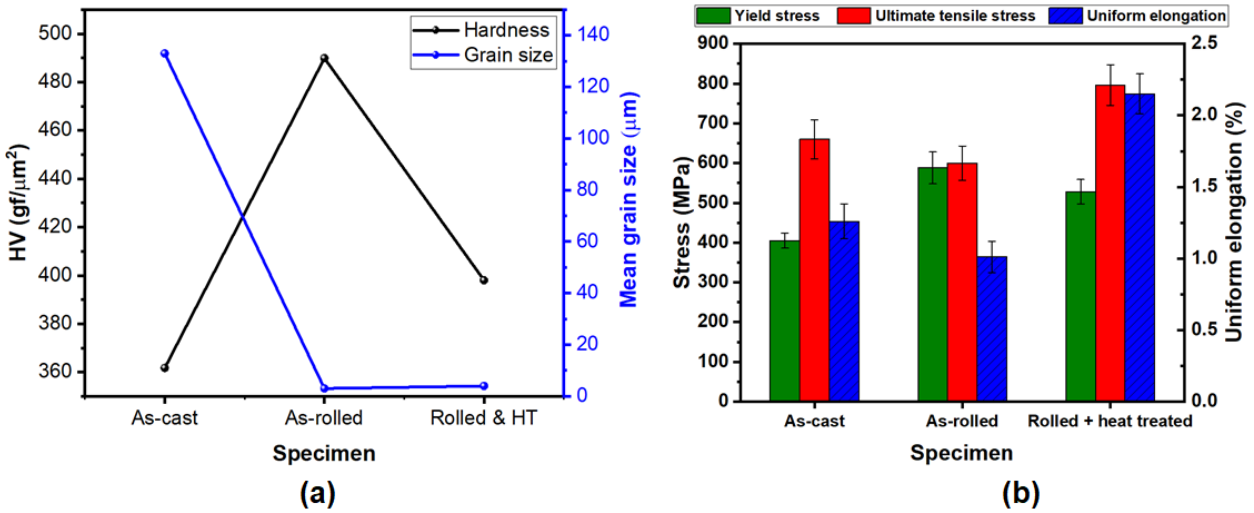

Fig. 10: Mechanical properties (a) micro-hardness and grain size, and (b) PIP estimation of the tensile properties under different processing conditions.

Table 1: The W-H crystallite size and lattice strains of the as-rolled and rolled + heat treated.

Specimen	Crystallite size (nm)	Lattice strain (ε)
As-rolled	1.2926	0.2183
Rolled + heat treated	11.2181	-0.0022

Table 2: Phase acquisition **[30]**

Phase name	a	b	c	α	β	γ	Space group
α_2 (Alpha 2)	5.73 Å	5.73 Å	4.64 Å	90.00°	90.00°	120.00°	194 (P63/mmc)
α_2 (Ti_3Al)	5.72 Å	5.72 Å	4.64 Å	90.00°	90.00°	120.00°	194 (P63/mmc)
γ (TiAl)	2.81 Å	2.81 Å	4.08 Å	90.00°	90.00°	90.00°	123 (P4/mmm)
Ti_5Si_3	7.45 Å	7.45 Å	5.14 Å	90.00°	90.00°	120.00°	193 (P63/mcm)

Conflict of interest

The authors declare that they have no known competing financial interests or personal relationships that could have appeared to influence the work reported in this paper.